ACS OMEGA

Article

Cite This: ACS Omega 2018, 3, 9360−9368

http://pubs.acs.org/journal/acsodf

Stable Platinum(IV) Corroles: Synthesis, Molecular Structure, and Room-Temperature Near-IR Phosphorescence

Abraham B. Alemayehu,[†] Laura J. McCormick,[‡] Kevin J. Gagnon,[‡] Sergey M. Borisov,[§] and Abhik Ghosh*[,†]

[†]Department of Chemistry, UiT—The Arctic University of Norway, N-9037 Tromsø, Norway

[‡]Advanced Light Source, Lawrence Berkeley National Laboratory, Berkeley, California 94720-8229, United States

[§]Institute of Analytical Chemistry and Food Chemistry, NAWI Graz, Graz University of Technology, Stremayrgasse 9, 8010 Graz, Austria

Supporting Information

ABSTRACT: A series of stable Pt(IV) corrole complexes with the general formula $Pt^{IV}[TpXPC](m/p\text{-}C_6H_4CN)(py)$, where $TpXPC^{3-}$ is the trianion of a tris(*p*-X-phenyl)corrole and X = CF_3, H, and CH_3, has been synthesized, affording key physicochemical data on a rare and elusive class of metallocorroles. Single-crystal X-ray structures of two of the complexes revealed very short equatorial Pt−N distances of 1.94−1.97 Å, an axial Pt−C distance of ∼2.03 Å, and an axial Pt−N distance of ∼2.22 Å. The complexes exhibit Soret maxima at ∼430 nm, which are essentially independent of the *meso*-aryl para substituents, and strong Q bands with the most intense peak at 595−599 nm. The substituent-independent Soret maxima are consistent with an innocent Pt^{IV}−$corrole^{3-}$ description for the complexes. The low reduction potentials (−1.45 ± 0.08 V vs saturated calomel reference electrode) also support a highly stable Pt(IV) ground state as opposed to a noninnocent $corrole^{\bullet 2-}$ description. The reductions, however, are irreversible, which suggests that they involve concomitant cleavage of the Pt−aryl bond. Unlike Pt(IV) porphyrins, two of the complexes, $Pt^{IV}[TpXPC](m\text{-}C_6H_4CN)(py)$ (X = CF_3 and CH_3), were found to exhibit room-temperature near-IR phosphorescence with emission maxima at 813 and 826 nm, respectively. The quantum yield of ∼0.3% is comparable to those observed for six-coordinate Ir(III) corroles.

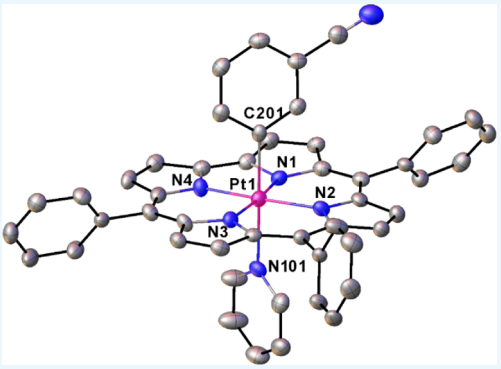

INTRODUCTION

The 5d metallocorroles constitute a unique class of size-mismatched complexes that incorporate a large 5d transition-metal ion within a sterically constrained macrocyclic ligand.[1] Despite a steric mismatch inherent in their structures, the majority of them exhibit remarkable chemical and photochemical stabilities. A number of them also exhibit room-temperature near-IR phosphorescence,[2] which has led to applications as oxygen sensors[3−5] and as photosensitizers in photodynamic therapy and dye-sensitized solar cells.[6,7] Platinum(IV) corroles, of which there has been only a single report,[8] are particularly intriguing because of their potential for axial reactivity. They are, however, only accessible via a low-yielding, serendipitously discovered reaction, which involves the interaction of a free-base corrole and $Pt_4(OAc)_8{\cdot}2HOAc$ in benzonitrile at high temperature. The initially formed Pt(IV) products, $Pt^{IV}[TpXPC](m/p\text{-}C_6H_4CN)(PhCN)$, where *TpXPC* is the trianion of a *meso*-tris(*para*-X-phenyl)corrole (X = CF_3, H, and CH_3) and the $m/p\text{-}C_6H_4CN$ group derives from the solvent (i.e., PhCN), proved unstable, but could be derivatized to stable, paramagnetic products $Pt^{IV}[TpXPC^{\bullet 2-}]^{\cdot}(m/p\text{-}C_6H_4CN)(Ar)$, which proved amenable to single-crystal X-ray structure determination.[8] Here, we report that in situ exposure of the initially formed Pt(IV)-PhCN products to pyridine leads to a new class of stable, nonradical Pt(IV) corroles with the general formula $Pt^{IV}[TpXPC](m/p\text{-}C_6H_4CN)(py)$, which have been variously characterized with single-crystal X-ray structure determination, electrochemical studies, and UV−vis−NIR absorption and emission spectroscopy (Figure 1). Although the results represent modest progress from a synthetic viewpoint, the physicochemical measurements afford significant insight into the electronic properties of a rare and elusive class of substances.

RESULTS AND DISCUSSION

As mentioned above, the Pt(IV) corroles $Pt^{IV}[TpXPC](m/p\text{-}C_6H_4CN)(py)$ (X = CF_3, H, and CH_3) were obtained rather simply by the addition of pyridine to the reaction mixture at the end of the Pt insertion. For all compounds, purity and composition were established via thin-layer chromatography,

Received: May 26, 2018
Accepted: August 1, 2018
Published: August 17, 2018

DOI: 10.1021/acsomega.8b01149
ACS Omega 2018, 3, 9360−9368

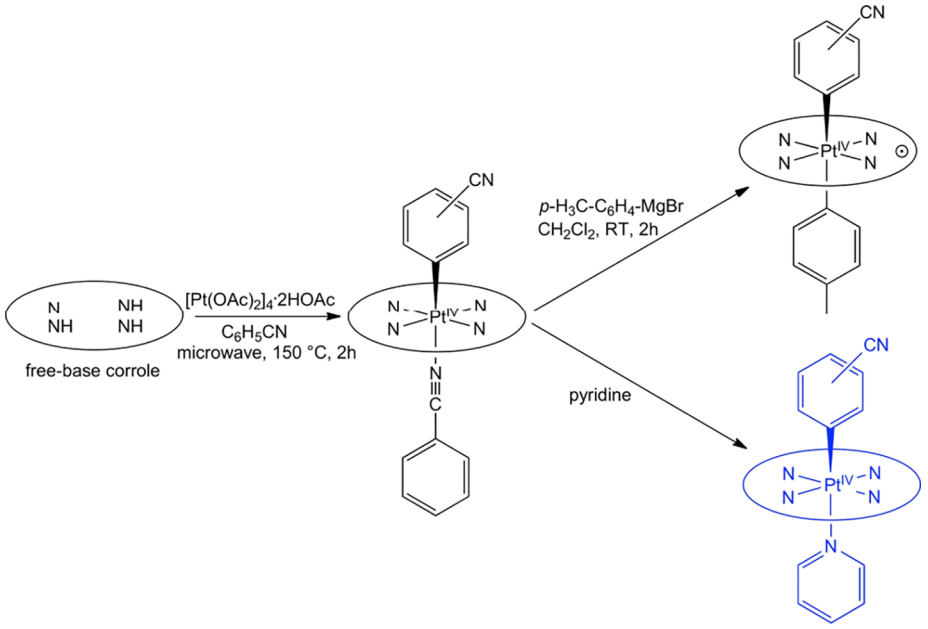

Figure 1. Current status of Pt−corrole chemistry; the complexes prepared in the course of this study are schematically depicted in blue.

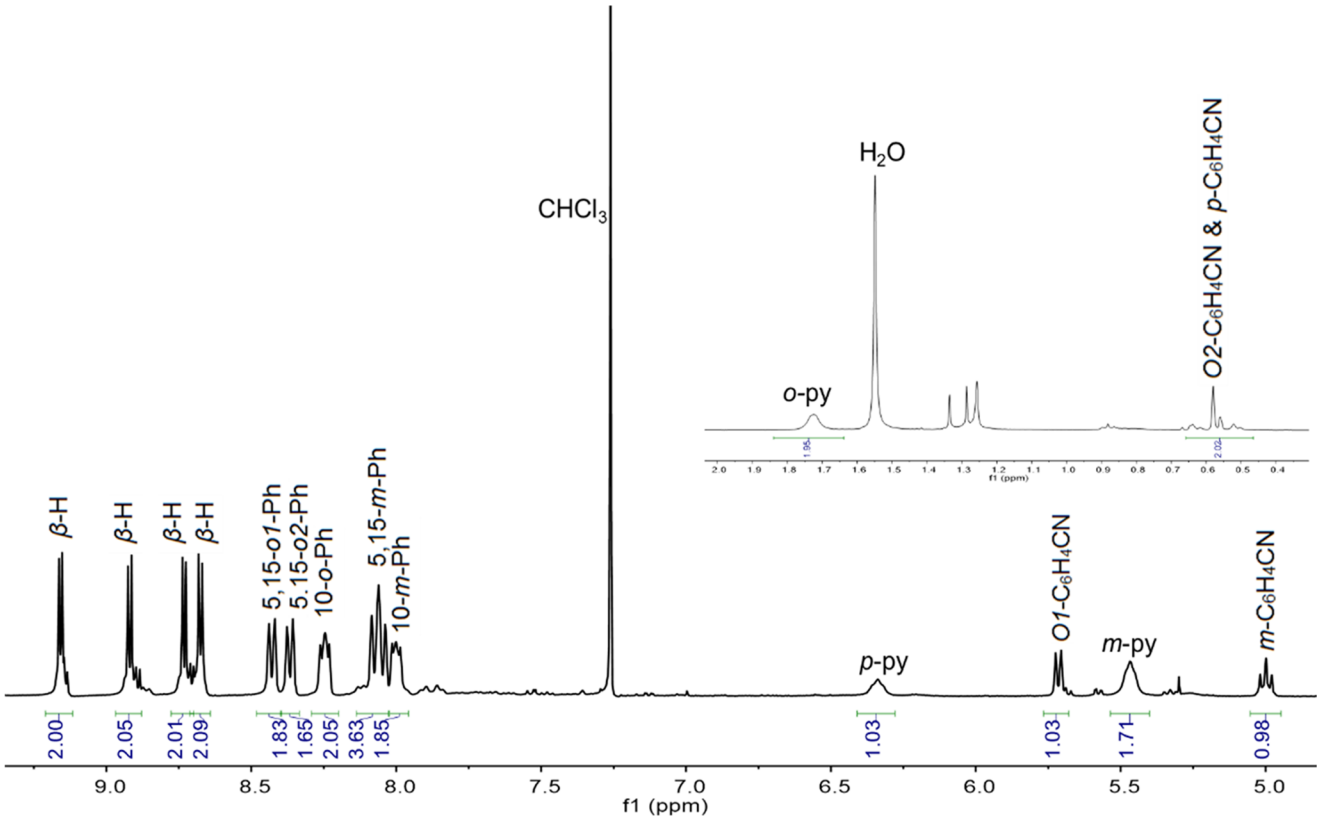

Figure 2. Representative ^{1}H NMR spectrum: Pt[T*p*CF$_3$PC](*m*-C$_6$H$_4$CN)(py).

high-resolution electrospray ionization mass spectrometry, and ^{1}H NMR spectroscopy (Figures 2 and 3). Elemental analyses, however, could not be obtained because of the very small quantities available. Single-crystal X-ray structures could be obtained for two of the complexes, providing unambiguous proof of structure (Table 1). Both structures revealed a Pt atom located exactly or nearly exactly in the mean plane of a planar corrole ligand. For Pt^{IV}[T*p*CF$_3$PC](*m*-C$_6$H$_4$CN)(py), the two axial ligands, *m*-C$_6$H$_4$CN and pyridine, were found to occupy symmetry-equivalent sites in the crystal, each with 50% occupancy, and were modeled such that the atoms of the two six-membered rings were superimposed (Figure 4). Accordingly, the axial Pt−C/N distances for this structure only represent an average of the "true" Pt−C and Pt−N distances. Fortunately, the second structure, Pt^{IV}[TPC](*m*-C$_6$H$_4$CN)(py) (TPC = triphenylcorrolato), was found to be fully

DOI: 10.1021/acsomega.8b01149
ACS Omega 2018, 3, 9360−9368

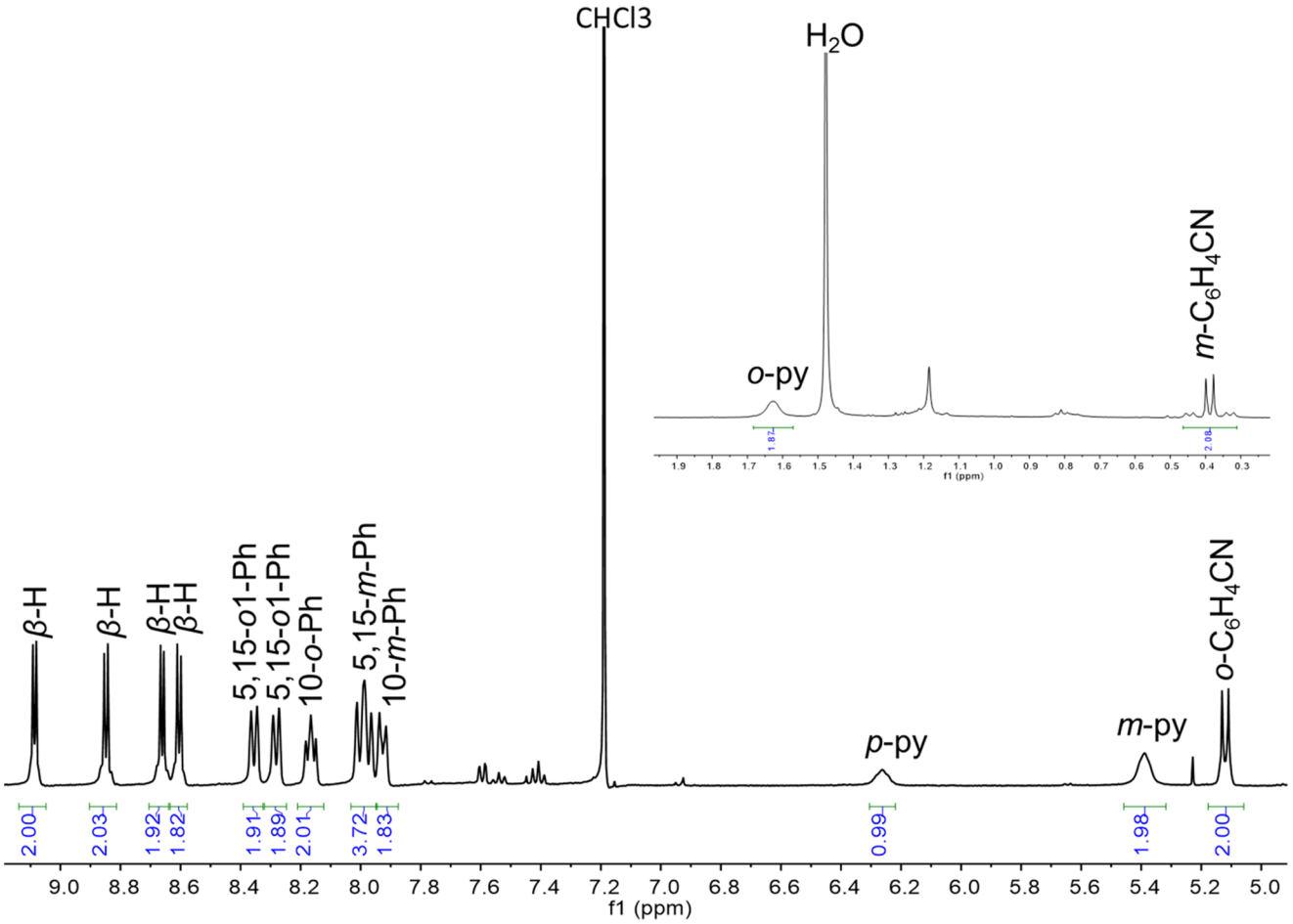

Figure 3. Representative ^{1}H NMR spectrum: Pt[T*p*CF$_3$PC](*p*-C$_6$H$_4$CN)(py).

ordered (Figure 5). The structures exhibit some of the shortest Pt−N distances known, which for the equatorial nitrogens are 1.955 ± 0.015 Å, reflecting the sterically constrained character of 5d metallocorroles. The axial Pt−C and Pt−N distances in the TPC complex are longer, 2.033(7) and 2.216(6) Å, respectively.

All six complexes exhibit slightly split Soret bands (Table 2 and Figures 6 and 7), which are essentially unaffected by the para substituents on the *meso*-aryl groups as well as strong Q bands. Over a long series of studies, we have shown that such substituent-insensitive Soret maxima are indicative of an innocent, nonradical corrole macrocycle, which is typical of the great majority of stable 4d and 5d metallocorroles, including MoO,[9] RuN,[10] OsN,[11] TcO,[12] ReO,[13] and Au[14−17] corroles as well as Mo[18] and W biscorroles.[19] In contrast, the Soret maxima of the Pt^{IV}[T*p*XPC$^{\bullet 2-}$](*m*/*p*-C$_6$H$_4$CN)(Ar) were found to redshift dramatically in response to increasing electron-donating character of the para substituent X,[7] a phenomenon that is also observed for other noninnocent metallocorroles, such as MnCl,[20,21] FeCl,[22,23] FeNO,[24,25] Fe$_2$(*μ*-O),[26] and Cu corroles.[27−35]

Cyclic voltammetry measurements were carried out for the *meta*-cyanophenyl series Pt^{IV}[T*p*XPC](*m*-C$_6$H$_4$CN)(py), which could be obtained in somewhat higher yields than the para series (Figure 8 and Table 2). Given the instability of the Pt(V) state, the oxidation potentials, which range from 0.56 V (for X = CH$_3$) to 0.74 V (for X = CF$_3$), may be safely assigned to corrole-centered oxidation. The low values of the reduction potentials, which range from −1.53 V (for X = CH$_3$) to −1.37 V (for X = CF$_3$), underscore the high stability of the Pt^{IV}Ar−corrole unit toward reduction. That said, although the electrochemical HOMO-LUMO gap of 2.1 eV is typically indicative of a redox-inactive metal center and of ligand-centered oxidation and reduction,[10−13,16,36] the fact that the reduction is irreversible suggests concomitant cleavage of the Pt−Ar bond.

Photophysical measurements were carried out on two of the complexes, Pt^{IV}[T*p*XPC](*m*-C$_6$H$_4$CN)(py) for X = CF$_3$ and CH$_3$ (Table 3 and Figures 9 and 10). Both are clearly phosphorescent, which was confirmed by almost complete quenching of the emission in the presence of oxygen (Figure 9b,d), measurement of the decay time (Figure 10) and by acquisition of luminescence excitation spectra (Figure 9a,c). The latter are essentially identical to the absorption spectra; the small deviations are due to nonlinearities ascribable to strong absorption in the Soret region (the concentration used was necessary for obtaining high-quality emission spectra with excitation in the Q-band). The NIR phosphorescence is rather weak, but the quantum yields are in the same order of magnitude as those observed for Ir(III) corroles.[2] This observation is interesting, considering that Pt(IV) porphyrins,[37] in contrast to Pt(II) porphyrins,[38−41] have been reported to be nonemissive.[42] Weak red fluorescence (not quenchable by oxygen) was also clearly detected for the two compounds studied. The quantum yields for the fluorescence were estimated to be about an order of magnitude lower than

DOI: 10.1021/acsomega.8b01149
ACS Omega 2018, 3, 9360−9368

Table 1. X-ray Crystallographic Data for the Two Crystals Analyzed[a]

sample	Pt[TPC](Ar)(py)	Pt[T*p*CF$_3$PC](Ar)(py)
chemical formula	$C_{49}H_{32}N_6Pt$	$C_{52}H_{29}F_9N_6Pt$
formula mass	899.89	1103.90
crystal system	triclinic	monoclinic
space group	$P\bar{1}$	$C2/c$
λ (Å)	0.7293	0.8857
a (Å)	9.4792(15)	18.9584(10)
b (Å)	12.0922(19)	16.8577(8)
c (Å)	16.675(3)	14.0096(7)
α (deg)	109.102(3)	90
β (deg)	95.415(3)	111.553(3)
γ (deg)	90.850(3)	90
Z	2	4
V (Å^3)	1795.9(5)	4164.3(4)
temperature (K)	173(2)	100(2)
density (g/cm^3)	1.664	1.761
measured reflections	47 230	20 649
unique reflections	11 271	4807
parameters	506	340
restraints	0	58
R_{int}	0.1151	0.0544
θ range (deg)	2.217−31.857	2.237−21.225
R_1, wR_2 all data	0.0583, 0.1336	0.0482, 0.0746
S (GooF) all data	1.033	1.037
max/min res. dens. (e/Å^3)	3.436/−1.496	0.968/−0.872

[a]Ar = *m*-C_6H_4CN.

those for the phosphorescence. Upconversion with a triplet annihilator, which proved feasible with OsN corroles,[4] was found to be very weak due to the relatively low energy of the triplet state and the short triplet state decay times.

CONCLUSIONS

In what is only the second report on platinum corroles, we have described the synthesis of the first set of stable Pt(IV) complexes, in which the corrole is thought to be an innocent ligand (i.e., without radical character). These have the general formula Pt^{IV}[T*p*XPC](*m*/*p*-C_6H_4CN)(py), where X = CF_3, H, and CH_3. Although the yields are low (typically <5%), the

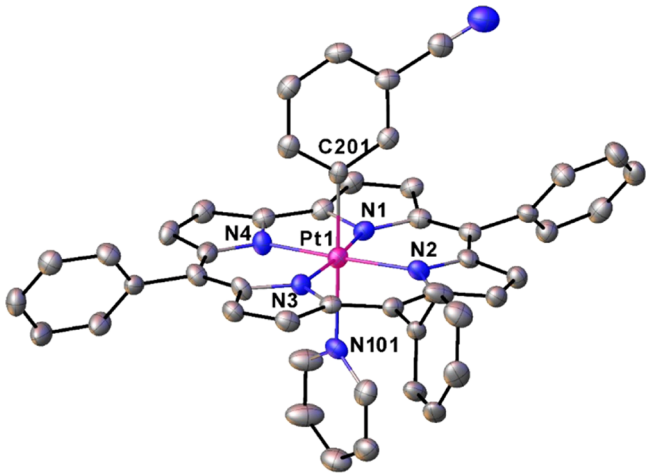

Figure 5. Selected distances (Å): Pt1−N1 1.944(5), Pt1−N2 1.966(5), Pt1−N3 1.955(6), Pt1−N4 1.944(5), Pt1−N101 2.216(6), and Pt1−C201 2.033(7).

compounds could be characterized with the standard spectroscopic methods and in two cases single-crystal X-ray crystallography providing rare insight into an elusive class of molecules. The structures revealed short equatorial Pt−N distance of 1.94−1.97 Å, an axial Pt−C distance of ∼2.03 Å, and an axial Pt−N distance of ∼2.22 Å. The UV−vis spectra revealed Soret maxima at ∼430 nm, which are essentially independent of the *meso*-aryl para substituents and strong Q bands with the most intense peak at 595−599 nm. The substituent-independent Soret maxima are consistent with an innocent Pt^{IV}−corrole^{3-} description for the new complexes. The low reduction potentials (−1.45 ± 0.08 V vs saturated calomel reference electrode (SCE)) also support a highly stable Pt(IV) ground state and rule out a corrole$^{\bullet 2-}$ description. The reductions, however, were found to be irreversible, which suggests that they involve concomitant cleavage of the Pt−aryl bond. Somewhat to our surprise and unlike Pt(IV) porphyrins, two of the complexes, Pt^{IV}[T*p*XPC]-(*m*-C_6H_4CN)(py) (X = CF_3 and CH_3), were found to exhibit room-temperature near-IR phosphorescence with emission maxima at 813 and 826 nm, respectively. The quantum yield of

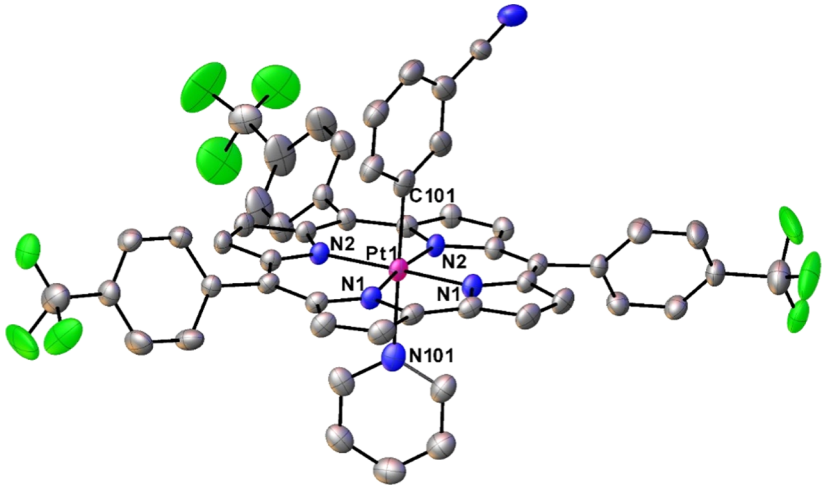

Figure 4. Thermal ellipsoid plot for Pt^{IV}[T*p*CF$_3$PC](*m*-C_6H_4CN)(py). Selected distances (Å): Pt1−N1 1.950(3), Pt1−N2 1.971(3), and Pt1−C/N101 2.148(4).

DOI: 10.1021/acsomega.8b01149
ACS Omega 2018, 3, 9360−9368

Table 2. Spectroscopic and Electrochemical Properties: UV−vis λ_{max} (nm) and $E_{1/2}$ Values (V) of Pt[T*p*XPC](*m*/*p*-C_6H_4CN)(py)

complex	λ_{max} (Soret)	λ_{max} (Q)	$E_{1/2(ox2)}$	$E_{1/2(ox1)}$	$E_{1/2(red1)}$	ΔE
Pt[T*p*CF_3PC](*m*-C_6H_4CN)(py)	430	569, 595	1.37	0.74	−1.37	2.11
Pt[TPC](*m*-C_6H_4CN)(py)	427, 437	567, 596	1.12	0.61	−1.49	2.10
Pt[T*p*CH_3PC](*m*-C_6H_4CN)(py)	427, 438	567, 599	1.11	0.56	−1.53	2.09
Pt[T*p*CF_3PC](*p*-C_6H_4CN)(py)	430	571, 595				
Pt[TPC](*p*-C_6H_4CN)(py)	427, 437	568, 597				
Pt[T*p*CH_3PC](*p*-C_6H_4CN)(py)	427, 438	567, 599				

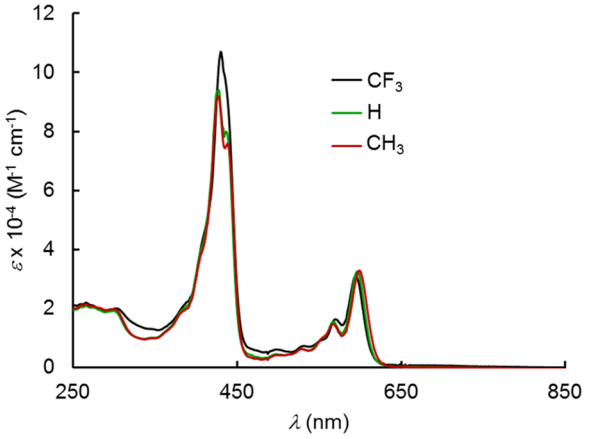

Figure 6. UV−vis spectra of Pt[T*p*XPC](*m*-C_6H_4CN)(py), X = CF_3, H, and CH_3.

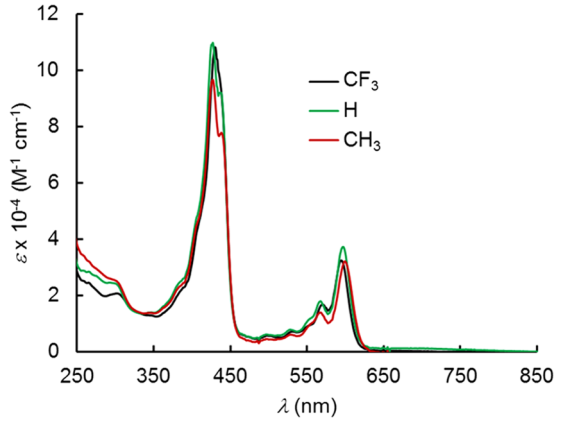

Figure 7. UV−vis spectra of Pt[T*p*XPC](*p*-C_6H_4CN)(py).

~0.3% is in the same order of magnitude as those of six-coordinate Ir(III) corroles.

EXPERIMENTAL SECTION

Materials. Free-base *meso*-triarylcorroles were synthesized according to a literature procedure.[43] Platinum(II) chloride was purchased from Sigma-Aldrich and used to synthesize tetranuclear platinum(II) acetate, as described in the literature.[44] Platinum insertion reactions were carried out in a Biotage microwave reactor using 20 mL of microwave vials. Silica gel 60 (0.04−0.063 mm particle size, 230−400 mesh, Merck) was used for flash chromatography, and silica gel 60 preparative thin-layer chromatography (PTLC) plates (20 cm × 20 cm, 0.5 mm thick, Merck) were used for final purification of all complexes.

Instrumental Methods. UV−visible−NIR spectra were recorded on an HP 8454 spectrophotometer. ^{1}H NMR spectra

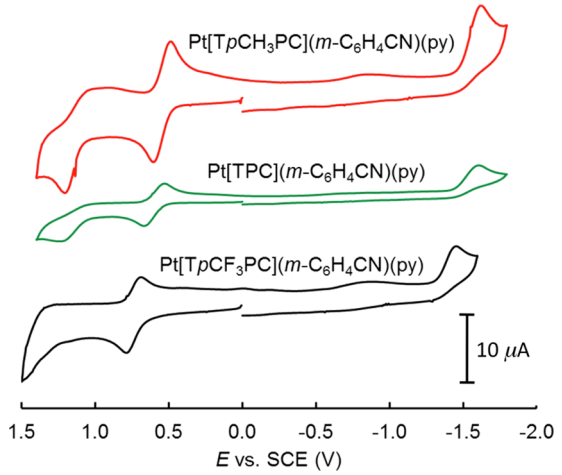

Figure 8. Cyclic voltammograms of Pt[T*p*XPC](*m*-C_6H_4CN)(py) (X = CF_3, H, and CH_3) in CH_2Cl_2 recorded at a scan rate of 100 mV/s.

Table 3. Summary of Photophysical Properties Measured in Deoxygenated Toluene at 25 °C

complex	$\lambda_{max,em}$ (nm)	Φ (%)	decay time (μs)
Pt^{IV}[T*p*CF_3PC](*m*-C_6H_4CN)(py)	813	0.27	22.9
Pt^{IV}[T*p*CH_3PC](*m*-C_6H_4CN)(py)	826	0.19	17.5

were recorded on 400 MHz Bruker AVANCE III HD spectrometer equipped with a 5 mm BB/^{1}H SmartProbe at 298 K in $CDCl_3$ and referenced to residual $CHCl_3$ at 7.26 ppm. Mass spectra were recorded on a Thermo Scientific LTQ Orbitrap XL spectrometer with an Ion-Max electrospray ion source.

Cyclic voltammetry was carried out at 298 K with an EG&G model 263A potentiostat having a three-electrode system: a glassy carbon working electrode, a platinum wire counter electrode, and a saturated calomel reference electrode (SCE). Anhydrous CH_2Cl_2 (Aldrich) was used as solvent and tetrakis(*n*-butyl)ammonium perchlorate, recrystallized twice from absolute ethanol and dried in a desiccator for at least 2 weeks, was used as the supporting electrolyte. The reference electrode was separated from the bulk solution using a fritted glass bridge filled with the solvent/supporting-electrolyte mixture. The electrolyte solution was purged with argon for at least 2 min, and all measurements were carried out under an argon blanket. All potentials were referenced to the SCE.

Emission and excitation spectra were acquired on a FluoroLog 3 spectrofluorometer (Horiba Scientific) equipped with a NIR-sensitive R2658 photomultiplier (Hamamatsu). Relative quantum yields at room temperature were estimated using a solution of Pt(II) tetraphenyltetrabenzoporphyrin in toluene as a reference (Φ = 21%).[40] The dye solutions were

DOI: 10.1021/acsomega.8b01149
ACS Omega 2018, 3, 9360−9368

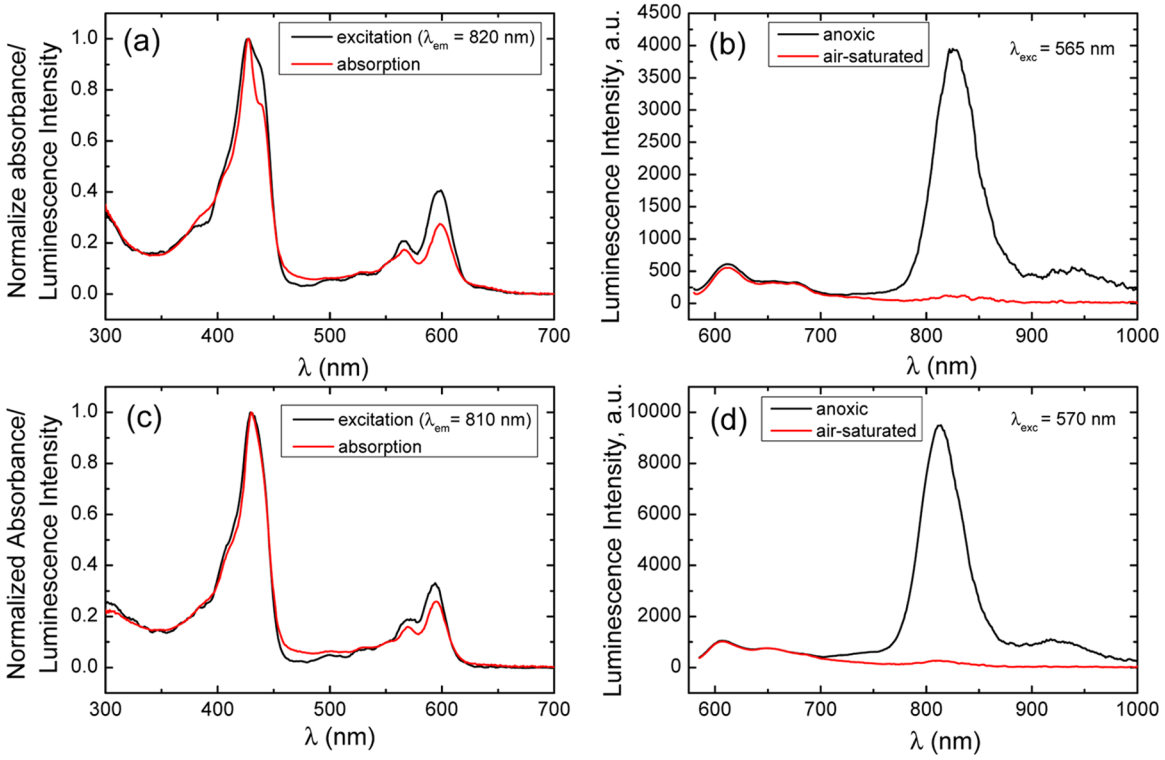

Figure 9. Optical properties of Pt(IV) corroles: (a, c) absorption and luminescence excitation spectra of the Pt^{IV}[T*p*CH_3PC](*m*-C_6H_4CN)(py) and Pt^{IV}[T*p*CF_3PC](*m*-C_6H_4CN)(py), respectively, in toluene solution at 25 °C; (b, d) luminescence spectra of Pt^{IV}[T*p*CH_3PC](*m*-C_6H_4CN)(py) and Pt^{IV}[T*p*CF_3PC](*m*-C_6H_4CN)(py), respectively, in toluene under anoxic and air-saturated conditions at 25 °C.

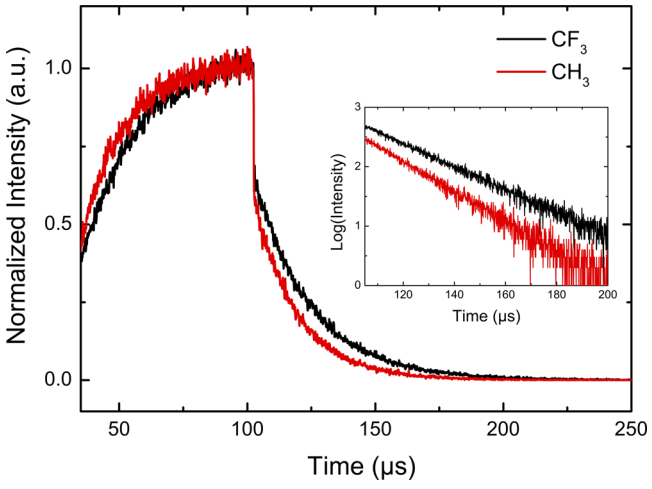

Figure 10. Phosphorescence decay for Pt(IV) corroles in anoxic toluene (25 °C, detected at 815 ± 7 nm).

deoxygenated in a screw-cap cuvette (Hellma, Mülheim, Germany) by bubbling argon through the solution for 12 min. Phosphorescence decay times were acquired in time domain on the FluoroLog 3 spectrofluorometer using a 390 nm SpectraLED (Horiba) as the excitation source.

General Procedure for the Synthesis of Pt[T*p*XPC](*m*/*p*-C_6H_4CN)(py), Where X = CF_3, H, CH_3. To a 20 mL microwave vial containing PhCN (5 mL) and a magnetic stirring bar were added a free-base corrole H_3[T*p*XPC] (0.114 mmol) and $Pt_4(OAc)_8$·2HOAc (1 equiv). The vial was sealed and heated for 2 h at 150 °C under microwave irradiation. Upon completion of the reaction, pyridine (0.5 mL) was added and the contents of the vial were transferred to a round-bottom flask (50 mL) and evaporated to dryness. The resulting solid was dissolved in dichloromethane (5 mL) and loaded onto a silica gel column and eluted with a mixture of dichloromethane and *n*-hexane (the exact ratio of which is stated below for each case). All fractions containing Pt[T*p*XPC](*m*/*p*-C_6H_4CN)(py), characterized by a Soret λ_{max} between 426 and 430 nm, were collected and evaporated to dryness. The product thus obtained was separated into the meta and para regioisomers with PTLC using a dichloromethane/*n*-hexane mixture as eluent, as indicated below.

Synthesis and Separation of Pt[T*p*CF_3PC](*m*/*p*-C_6H_4CN)(py). The crude reaction product was chromatographed on a silica gel column with 3:2 dichloromethane/*n*-hexane as eluent. The fractions with a UV−vis λ_{max} of 430 nm were collected and evaporated to dryness, resulting in a combined yield of 3.69 mg (6.6%) for the Pt[T*p*CF_3PC](*m*/*p*-C_6H_4CN)(py) regioisomers. PTLC with 1:1 dichloromethane/*n*-hexane as eluent was then used to separate the m- and p-isomers; the top band was identified as Pt[T*p*CF_3PC](*m*-C_6H_4CN)(py) and the lower band as Pt[T*p*CF_3PC](*p*-C_6H_4CN)(py) based on ^{1}H NMR analysis. Dark purple X-ray quality crystals of the meta isomer were grown by slow evaporation of a dichloromethane/*n*-hexane solution of the complex over a period of 15 days. Spectroscopic characterization data for the two isomers are as follows (see also Figures 2 and 3).

Pt[T*p*CF_3PC](*m*-C_6H_4CN)(py). Yield 2.15 mg (3.52%). UV−vis (CH_2Cl_2) λ_{max} (nm, $\varepsilon \times 10^{-4}$ M^{-1} cm^{-1}): 430 (10.70), 498 (0.60), 531 (0.72), 569 (1.62), 595 (3.08). ^{1}H NMR δ: 9.16 (d, 2H, $^3J_{HH}$ = 4.08 Hz, β-H); 8.92 (d, 2H, $^3J_{HH}$ = 4.60 Hz, β-H); 8.73 (d, 2H, $^3J_{HH}$ = 4.04 Hz, β-H); 8.68 (d, 2H, $^3J_{HH}$ = 5.12 Hz, β-H); 8.43 (d, 2H, $^3J_{HH}$ = 8.12 Hz, 5,15-*o*1-Ph); 8.37 (d, 2H, $^3J_{HH}$ = 7.60 Hz, 5,15-*o*2-Ph); 8.25

DOI: 10.1021/acsomega.8b01149
ACS Omega 2018, 3, 9360−9368

(overlapping doublets, 2H, $^3J_{HH}$ = 8.12 Hz, 10-*o*1-Ph and 10-*o*2-Ph); 8.07 (overlapping doublets, 4H, $^3J_{HH}$ = 7.60 Hz, 5,15-*m*1-Ph and 5,15-*m*2-Ph); 8.00 (overlapping doublets, 2H, $^3J_{HH}$ = 8.12 Hz, 10-*m*1-Ph and 10-*m*2-Ph); 6.34 (br s, 1H, 4-py); 5.72 (d, 1H, $^3J_{HH}$ = 7.44 Hz, C_6H_4CN *ortho*1); 5.47 (br s, 2H, 3,5-py); 5.00 (t, 1H, C_6H_4CN *meta*); 1.73 (br s, 2H, 2,6-py), 0.57 (d, 1H, C_6H_4CN *para*; overlapping with s, 1H, C_6H_4CN *ortho*2). High-resolution mass spectrometry (HRMS) (major isotopomer): M^+ = 1103.2123 (expt), 1103.1952 (calcd for $C_{52}H_{29}N_6F_9Pt$).

Pt[T*p*CF$_3$PC](*p*-C$_6$H$_4$CN)(py). Yield 1.12 mg (1.83%). UV−vis (CH_2Cl_2) λ_{max} (nm, $\varepsilon \times 10^{-4}$ M^{-1} cm^{-1}): 430 (10.82), 498 (0.56), 531 (0.70), 571 (1.64), 595 (3.23). ^1H NMR δ: 9.16 (d, 2H, $^3J_{HH}$ = 3.68 Hz, β-H); 8.92 (d, 2H, $^3J_{HH}$ = 5.20 Hz, β-H); 8.73 (d, 2H, $^3J_{HH}$ = 4.28 Hz, β-H); 8.68 (d, 2H, $^3J_{HH}$ = 5.02 Hz, β-H); 8.43 (d, 2H, $^3J_{HH}$ = 7.96 Hz, 5,15-*o*1-Ph); 8.35 (d, 2H, $^3J_{HH}$ = 7.96 Hz, 5,15-*o*2-Ph); 8.24 (overlapping doublets, 2H, $^3J_{HH}$ = 8.12 Hz, 10-*o*1-Ph and 10-*o*2-Ph); 8.06 (d, 4H, $^3J_{HH}$ = 8.12 Hz, 5,15-*m*1-Ph and 5,15-*m*2-Ph); 8.00 (overlapping doublets, 2H, $^3J_{HH}$ = 8 Hz, 10-*m*1-Ph and 10-*m*2-Ph); 6.33 (br s, 1H, 4-py); 5.46 (br s, 2H, 3,5-py); 5.19 (d, 2H, $^3J_{HH}$ = 6.88 Hz, C_6H_4CN *ortho*); 1.70 (br s, 2H, 2,6-py), 0.46 (d, 2H, $^3J_{HH}$ = 8.16 Hz, C_6H_4CN *meta*). HRMS (major isotopomer): M^+ = 1103.2118 (expt), 1103.1952 (calcd for $C_{52}H_{29}N_6F_9Pt$).

Synthesis and Separation of Pt[TPC](*m*/*p*-C$_6$H$_4$CN)(py). The crude reaction product was initially chromatographed on a silica gel column with 2:1 dichloromethane/*n*-hexane as eluent. The fractions with a λ_{max} of 427 nm were collected and evaporated to dryness, resulting in combined yield of 3.59 mg (7.2%) for the Pt(TPC)(*m*/*p*-C_6H_4CN)(PhCN) regioisomers. PTLC with 3:2 dichloromethane/*n*-hexane as eluent was then used to separate the isomers; the top band was identified as Pt[TPC](*m*-C_6H_4CN)(py) and the lower band as Pt[TPC](*p*-C_6H_4CN)(py) based on ^1H NMR analysis.

Pt[TPC](*m*-C$_6$H$_4$CN)(py). Yield 2.1 mg (4.21%). UV−vis (CH_2Cl_2) λ_{max} (nm, $\varepsilon \times 10^{-4}$ M^{-1} cm^{-1}): 427 (9.41), 437 (7.99), 496 (0.46), 528 (0.64), 567 (1.56), 596 (3.25). ^1H NMR δ: 9.09 (d, 2H, $^3J_{HH}$ = 4.88 Hz, β-H); 8.93 (d, 2H, $^3J_{HH}$ = 4.88 Hz, β-H); 8.73 (d, 2H, $^3J_{HH}$ = 4.88 Hz, β-H); 8.67 (d, 2H, $^3J_{HH}$ = 4.24 Hz, β-H); 8.32 (d, 2H, $^3J_{HH}$ = 6.80 Hz, 5,15-*o*1); 8.24 (d, 2H, $^3J_{HH}$ = 6.56 Hz, 5,15-*o*2); 8.10 (overlapping doublets, 2H, $^3J_{HH}$ = 8.12 Hz, 10-*o*1 and 10-*o*2); 7.68−7.83 (m, 9H, overlapping 5,10,15-*m*-Ph and 5,10,15-*p*-Ph); 6.29 (br s, 1H, 4-py); 5.70 (d, 1H, $^3J_{HH}$ = 6.92 Hz, C_6H_4CN *ortho*1); 5.43 (br s, 2H, 3,5-py); 4.99 (t, 1H, $^3J_{HH}$ = 6.92 Hz, C_6H_4CN *meta*); 1.79 (br d, 2H, 2,6-py), 0.68 (d, 1H, C_6H_4CN *para* overlapping with s, 1H, C_6H_4CN *ortho*2). HRMS (major isotopomer): M^+ = 899.2327 (expt), 899.2331 (calcd for $C_{49}H_{32}N_6Pt$).

Pt[TPC](*p*-C$_6$H$_4$CN)(py). Yield 1.08 mg (2.16%). UV−vis (CH_2Cl_2) λ_{max} (nm, $\varepsilon \times 10^{-4}$ M^{-1} cm^{-1}): 427 (10.98), 437 (9.02), 496 (0.61), 528 (0.78), 568 (1.78), 597 (3.72). ^1H NMR δ: 9.08 (d, 2H, $^3J_{HH}$ = 4.28 Hz, β-H); 8.92 (d, 2H, $^3J_{HH}$ = 4.92 Hz, β-H); 8.73 (d, 2H, $^3J_{HH}$ = 4.32 Hz, β-H); 8.66 (d, 2H, $^3J_{HH}$ = 4.28 Hz, β-H); 8.31 (d, 2H, $^3J_{HH}$ = 7.96 Hz, 5,15-*o*1-Ph); 8.24 (d, 2H, $^3J_{HH}$ = 6.88 Hz, 5,15-*o*2-Ph); 8.10 (overlapping doublets, 2H, $^3J_{HH}$ = 8.12 Hz, 10-*o*1-Ph and 10-*o*2-Ph); 7.83−7.68 (m, 9H, overlapping 5,10,15-*m*-Ph and 5,10,15-*p*-Ph); 6.30 (br s, 1H, 4-py); 5.43 (br s, 2H, 3-py); 5.19 (d, 2H, $^3J_{HH}$ = 6.80 Hz C_6H_4CN *ortho*); 1.77 (br s, 2H, 2,6-py); 0.56 (d, 2H, $^3J_{HH}$ = 6.08 Hz, C_6H_4CN *meta*). HRMS (major isotopomer): M^+ = 899.2331 (expt), 899.2331 (calcd for $C_{49}H_{32}N_6Pt$).

Synthesis and Separation of Pt[T*p*CH$_3$PC](*m*/*p*-C$_6$H$_4$CN)(py). The crude reaction product was chromatographed on a silica gel column with 3:1 dichloromethane/*n*-hexane as eluent. The fractions with a λ_{max} of 427 nm were collected and evaporated to dryness, resulting in combined yield of 4.17 mg (8.0%) for the Pt[T*p*CH_3PC](*m*/*p*-C_6H_4CN)(py) regioisomers. PTLC with 3:1 dichloromethane/*n*-hexane as eluent was then used to separate the isomers; the top band was identified as Pt[T*p*CH_3PC](*p*-C_6H_4CN)(py) and the lower band as Pt[T*p*CH_3PC](*m*-C_6H_4CN)(py) based on ^1H NMR analysis.

Pt[T*p*CH$_3$PC](*m*-C$_6$H$_4$CN)(py). Yield 2.3 mg (4.41%). UV−vis (CH_2Cl_2) λ_{max} (nm, $\varepsilon \times 10^{-4}$ M^{-1} cm^{-1}): 427 (9.19), 438 (7.59), 498 (0.41), 528 (0.62), 567 (1.47), 599 (3.28). ^1H NMR δ: 9.06 (d, 2H, $^3J_{HH}$ = 4.40 Hz, β-H); 8.92 (d, 2H, $^3J_{HH}$ = 4.36 Hz, β-H); 8.72 (d, 2H, $^3J_{HH}$ = 4.44 Hz, β-H); 8.66 (d, 2H, $^3J_{HH}$ = 4.40 Hz, β-H); 8.21 (d, 2H, $^3J_{HH}$ = 7.96 Hz, 5,15-*o*1-Ph); 8.12 (d, 2H, $^3J_{HH}$ = 6.68 Hz, 5,15-*o*2-Ph); 7.98 (overlapping doublets, 2H, $^3J_{HH}$ = 8.24 Hz, 10-*o*1-Ph and 10-*o*2-Ph); 7.60 (d, 2H, $^3J_{HH}$ = 8.24 Hz, 5,15-*m*1-Ph); 7.57 (d, 2H, $^3J_{HH}$ = 7.96 Hz, 5,15-*m*2-Ph); 7.51 (overlapping doublets, 2H, $^3J_{HH}$ = 8.12 Hz, 10-*m*1-Ph and 10-*m*2-Ph); 6.28 (br s, 1H, 4-py); 5.69 (d, 1H, $^3J_{HH}$ = 6.84 Hz, C_6H_4CN *ortho*1); 5.42 (br s, 2H, 3-py); 4.98 (t, 1H, $^3J_{HH}$ = 8.36 Hz, C_6H_4CN *meta*); 2.69 (s, 6H, 5,15-*p*-CH_3); 2.65 (s, 3H, 10-*p*-CH_3); 1.79 (br s, 2H, 2,6-py), 0.69 (d, 1H, C_6H_4CN *para* and s, 1H, C_6H_4CN *ortho*2). HRMS (major isotopomer): M^+ = 941.2897 (expt), 941.2800 (calcd for $C_{52}H_{38}N_6Pt$).

Pt[T*p*CH$_3$PC](*p*-C$_6$H$_4$CN)(py). Yield 1.17 mg (2.22%). UV−vis (CH_2Cl_2) λ_{max} (nm, $\varepsilon \times 10^{-4}$ M^{-1} cm^{-1}): 427 (9.67), 438 (7.79), 496 (0.46), 528 (0.62), 567 (1.40), 599 (3.21). ^1H NMR δ: 9.06 (d, 2H, $^3J_{HH}$ = 4.16 Hz, β-H); 8.92 (d, 2H, $^3J_{HH}$ = 3.80 Hz, β-H); 8.72 (d, 2H, $^3J_{HH}$ = 4.16 Hz, β-H); 8.66 (d, 2H, $^3J_{HH}$ = 5.20 Hz, β-H); 8.21 (d, 2H, $^3J_{HH}$ = 8.00 Hz, 5,15-*o*1-Ph); 8.12 (d, 2H, $^3J_{HH}$ = 8.68 Hz, 5,15-*o*2-Ph); 7.98 (overlapping doublets, 2H, $^3J_{HH}$ = 8.64 Hz, 10-*o*1-Ph and 10-*o*2-Ph); 7.60 (d, 2H, $^3J_{HH}$ = 8.64 Hz, 5,15-*m*1-Ph); 7.57 (d, 2H, $^3J_{HH}$ = 7.96 Hz, 5,15-*m*2-Ph); 7.51 (overlapping doublets, 2H, $^3J_{HH}$ = 7.96 Hz, 10-*m*1-Ph and 10-*m*2-Ph); 6.29 (br s, 1H, 4-py); 5.42 (br s, 2H, 3,5-py); 5.18 (d, 2H, $^3J_{HH}$ = 6.80 Hz, C_6H_4CN *ortho*); 2.69 (s, 6H, 5,15-*p*-CH_3); 2.65 (s, 3H, 10-*p*-CH_3); 1.76 (br s, 2H, 2,6-py), 0.57 (d, 2H, C_6H_4CN *meta*). HRMS (major isotopomer): M^+ = 941.2897 (expt), 941.2800 (calcd for $C_{52}H_{38}N_6Pt$).

X-ray Crystallographic Analyses. X-ray data for Pt[TPC](*m*-C_6H_4CN)(py) and Pt[T*p*CF_3PC](*m*-C_6H_4CN)(py) were collected on beamline 11.3.1 at the Advanced Light Source, Lawrence Berkeley National Laboratory. Each crystal was mounted on a MiTeGen Kapton loop and placed in a nitrogen cold stream provided by an Oxford Cryostream 800 Plus low-temperature apparatus on the goniometer head of a Bruker D8 diffractometer. The diffractometer was equipped with a PHOTON 100 CMOS detector for Pt[TPC](*m*-C_6H_4CN)(py) and a PHOTONII CPAD detector for Pt[T*p*CF_3PC](*m*-C_6H_4CN)(py), each operating in shutterless mode. Diffraction data were collected with synchrotron radiation monochromated using silicon (111) to a wavelength of 0.7293(1) Å for Pt[TPC](*m*-C_6H_4CN)(py) and 0.7749(1) Å for Pt[T*p*CF_3PC](*m*-C_6H_4CN)(py). An approximate full sphere of data was collected on each crystal using a combination of ϕ and ω scans. The crystals of Pt[TPC](*m*-

DOI: 10.1021/acsomega.8b01149
ACS Omega 2018, 3, 9360−9368

C_6H_4CN)(py) were found to be twinned, the components were separated using the CELL_NOW program.[45] Absorption corrections were applied with SADABS[46] for Pt[T*p*CF_3PC](*m*-C_6H_4CN)(py) and with TWINABS[47] for Pt[TPC](*m*-C_6H_4CN)(py). The structures were solved by intrinsic phasing (SHELXT)[48] and refined by full-matrix least squares on F^2 (SHELXL-2014)[49] using the ShelXle GUI.[50] All non-hydrogen atoms were refined anisotropically. Hydrogen atoms were geometrically calculated and refined as riding atoms.

The two axial ligands in Pt[T*p*CF_3PC](*m*-C_6H_4CN)(py), pyridine and C_6H_4CN, were found to occupy symmetry-equivalent sites within the crystal, each with 50% occupancy, and were modeled such that the atoms of the two six-membered rings were superimposed. The C and N atoms that coordinate to the Pt center (C101 and N101) were constrained to have identical *x*, *y*, and *z* coordinates via the EXYZ command in SHELX and were refined under separate PART instructions. Each of the remaining five atoms of the aromatic ring was modeled as common to both orientations with full occupancies, since attempts to independently model the two rings were unsuccessful. The CN and H substituents bound to C105 were refined under the same PART instructions as C101 and N101, respectively. The disordered axial ligands led to disorder in the unique $C_6H_4CF_3$ substituent, causing the CF_3 group to be positionally disordered over two symmetry-equivalent sites. The atoms belonging to this CF_3 group were refined with an occupancy of 0.5, but no attempt was made to model disorder in the aromatic ring of this substituent. Rotational disorder was also found for the CF_3 groups on the other two $C_6H_4CF_3$ substituents, and each CF_3 group was accordingly modeled over two orientations with complementary occupancies. Equivalent disordered atoms (e.g., N101/C101) were constrained to have equal U_{ij} values via the EADP command in SHELX. Additional crystallographic information has been summarized in Table 1, and full details can be found in the Crystallographic Information File provided as Supporting Information.

■ ASSOCIATED CONTENT

Supporting Information

The Supporting Information is available free of charge on the ACS Publications website at DOI: 10.1021/acsomega.8b01149.

Electrospray ionization mass spectra (PDF)

Crystal structures reported in this paper have been deposited at the Cambridge Crystallographic Data Centre and assigned the deposition numbers CCDC 1846980-1846981 (CIF)

■ AUTHOR INFORMATION

Corresponding Author

*E-mail: abhik.ghosh@uit.no.

ORCID

Laura J. McCormick: 0000-0002-6634-4717
Sergey M. Borisov: 0000-0001-9318-8273
Abhik Ghosh: 0000-0003-1161-6364

Notes

The authors declare no competing financial interest.

■ ACKNOWLEDGMENTS

This work was supported by NANO2021 grant no. 262229 of the Research Council of Norway (A.G.) and used resources of the Advanced Light Source, which is a DOE Office of Science User Facility under contract no. DE-AC02-05CH11231.

■ REFERENCES

(1) Ghosh, A. Electronic Structure of Corrole Derivatives: Insights from Molecular Structures, Spectroscopy, Electrochemistry, and Quantum Chemical Calculations. *Chem. Rev.* **2017**, *117*, 3798−3881.

(2) Palmer, J. H.; Durrell, A. C.; Gross, Z.; Winkler, J. R.; Gray, H. B. Near-IR Phosphorescence of Iridium(III) Corroles at Ambient Temperature. *J. Am. Chem. Soc.* **2010**, *132*, 9230−9231.

(3) Sinha, W.; Ravotto, L.; Ceroni, P.; Kar, S. NIR-Emissive Iridium(III) Corrole Complexes as Efficient Singlet Oxygen Sensitizers. *Dalton Trans.* **2015**, *44*, 17767−17773.

(4) Borisov, S. M.; Alemayehu, A.; Ghosh, A. Osmium-Nitrido Corroles as NIR Indicators for Oxygen Sensors and Triplet Sensitizers for Organic Upconversion and Singlet Oxygen Generation. *J. Mater. Chem. C* **2016**, *4*, 5822−5828.

(5) Lemon, C. M.; Powers, D. C.; Brothers, P. J.; Nocera, D. G. Gold Corroles as Near-IR Phosphors for Oxygen Sensing. *Inorg. Chem.* **2017**, *56*, 10991−10997.

(6) Alemayehu, A. B.; Day, N. U.; Mani, T.; Rudine, A. B.; Thomas, K. E.; Gederaas, O. A.; Vinogradov, S. A.; Wamser, C. C.; Ghosh, A. Gold Tris(carboxyphenyl)corroles as Multifunctional Materials: Room Temperature Near-IR Phosphorescence and Applications to Photodynamic Therapy and Dye-Sensitized Solar Cells. *ACS Appl. Mater. Interfaces* **2016**, *8*, 18935−18942.

(7) Teo, R. D.; Hwang, J. Y.; Termini, J.; Gross, Z.; Gray, H. B. Fighting Cancer with Corroles. *Chem. Rev.* **2016**, *117*, 2711−2729.

(8) Alemayehu, A. B.; Vazquez-Lima, H.; Beavers, C. M.; Gagnon, K. J.; Bendix, J.; Ghosh, A. Platinum Corroles. *Chem. Commun.* **2014**, *50*, 11093−11096.

(9) Johansen, I.; Norheim, H.-K.; Larsen, S.; Alemayehu, A. B.; Conradie, J.; Ghosh, A. Substituent Effects on Metallocorrole Spectra: Insights from Chromium-Oxo and Molybdenum-Oxo Triarylcorroles. *J. Porphyrins Phthalocyanines* **2011**, *15*, 1335−1344.

(10) Alemayehu, A. B.; Vazquez-Lima, H.; Gagnon, K. J.; Ghosh, A. Stepwise Deoxygenation of Nitrite as a Route to Two Families of Ruthenium Corroles: Group 8 Periodic Trends and Relativistic Effects. *Inorg. Chem.* **2017**, *56*, 5285−5294.

(11) Alemayehu, A. B.; Gagnon, K. J.; Terner, J.; Ghosh, A. Oxidative Metalation as a Route to Size-Mismatched Macrocyclic Complexes: Osmium Corroles. *Angew. Chem., Int. Ed.* **2014**, *53*, 14411−14414.

(12) Alemayehu, A. B.; Vazquez-Lima, H.; Gagnon, K. J.; Ghosh, A. Stepwise Deoxygenation of Nitrite as a Route to Two Families of Ruthenium Corroles: Group 8 Periodic Trends and Relativistic Effects. *Inorg. Chem.* **2017**, *56*, 5285−5294.

(13) Einrem, R. F.; Gagnon, K. J.; Alemayehu, A. B.; Ghosh, A. Metal-Ligand Misfits: Facile Access to Rhenium-Oxo Corroles by Oxidative Metalation. *Chem. − Eur. J.* **2016**, *22*, 517−520.

(14) Alemayehu, A. B.; Ghosh, A. Gold Corroles. *J. Porphyrins Phthalocyanines* **2011**, *15*, 106−110.

(15) Rabinovich, E.; Goldberg, I.; Gross, Z. Gold(I) and Gold(III) Corroles. *Chem. − Eur. J.* **2011**, *17*, 12294−12301.

(16) Thomas, K. E.; Alemayehu, A. B.; Conradie, J.; Beavers, C.; Ghosh, A. Synthesis and Molecular Structure of Gold Triarylcorroles. *Inorg. Chem.* **2011**, *50*, 12844−12851.

(17) Thomas, K. E.; Vazquez-Lima, H.; Fang, Y.; Song, Y.; Gagnon, K. J.; Beavers, C. M.; Kadish, K. M.; Ghosh, A. Ligand Noninnocence in Coinage Metal Corroles: A Silver Knife-Edge. *Chem. − Eur. J.* **2015**, *21*, 16839−16847.

(18) Alemayehu, A.; Vazquez-Lima, H.; McCormick, L. J.; Ghosh, A. Relativistic effects in metallocorroles: comparison of molybdenum and tungsten biscorroles. *Chem. Commun.* **2017**, *53*, 5830−5833.

DOI: 10.1021/acsomega.8b01149
ACS Omega 2018, 3, 9360−9368

(19) Alemayehu, A.; Vazquez-Lima, H.; Gagnon, K. J.; Ghosh, A. Tungsten Biscorroles: New Chiral Sandwich Compounds. *Chem. – Eur. J.* **2016**, *22*, 6914–6920.
(20) Steene, E.; Wondimagegn, T.; Ghosh, A. Resonance Raman Spectroscopy and Density Functional Theoretical Calculations of Manganese Corroles. A Parallelism between High-Valent Metallocorroles and Metalloporphyrins, Relevant to Horseradish Peroxidase and Chloroperoxidase Compound I and II Intermediates. *J. Inorg. Biochem.* **2002**, *88*, 113–118.
(21) Ganguly, S.; McCormick, L. J.; Conradie, J.; Gagnon, K. J.; Sarangi, R.; Ghosh, A. Electronic Structure of Manganese Corroles Revisited: X-ray structures, Optical and X-ray Absorption Spectroscopies, and Electrochemistry as Probes of Ligand Noninnocence. *Inorg. Chem.* **2018**. DOI: 10.1021/acs.inorgchem.8b00537.
(22) (a) Steene, E.; Wondimagegn, T.; Ghosh, A. Electrochemical and Electronic Absorption Spectroscopic Studies of Substituent Effects in Iron(IV) and Manganese(IV) Corroles. Do the Compounds Feature High-Valent Metal Centers or Noninnocent Corrole Ligands? Implications for Peroxidase Compound I and II Intermediates. *J. Phys. Chem. B* **2001**, *105*, 11406–11413; Addition/correction: (b) Steene, E.; Wondimagegn, T.; Ghosh, A. Electrochemical and Electronic Absorption Spectroscopic Studies of Substituent Effects in Iron(IV) and Manganese(IV) Corroles. Do the Compounds Feature High-Valent Metal Centers or Noninnocent Corrole Ligands? Implications for Peroxidase Compound I and II. *J. Phys. Chem. B* **2002**, *106*, 5312.
(23) Ganguly, S.; Giles, L. J.; Thomas, K. E.; Sarangi, R.; Ghosh, A. Ligand Noninnocence in Iron Corroles: Insights from Optical and X-ray Absorption Spectroscopies and Electrochemical Redox Potentials. *Chem. – Eur. J.* **2017**, *23*, 15098–15106.
(24) Vazquez-Lima, H.; Norheim, H. K.; Einrem, R. F.; Ghosh, A. Cryptic Noninnocence: FeNO Corroles in a New Light. *Dalton Trans.* **2015**, *44*, 10146–10151.
(25) Norheim, H.-K.; Capar, J.; Einrem, R. F.; Gagnon, K. J.; Beavers, C. M.; Vazquez-Lima, H.; Ghosh, A. Ligand Noninnocence in FeNO Corroles: Insights from β-Octabromocorrole Complexes. *Dalton Trans.* **2016**, *45*, 681–689.
(26) Ganguly, S.; Vazquez-Lima, H.; Ghosh, A. Wolves in Sheep's Clothing: μ-Oxo-Diiron Corroles Revisited. *Chem. – Eur. J.* **2016**, *22*, 10336–10340.
(27) Wasbotten, I. H.; Wondimagegn, T.; Ghosh, A. Electronic Absorption, Resonance Raman, and Electrochemical Studies of Planar and Saddled Copper(III) *Meso*-Triarylcorroles. Highly Substituent-Sensitive Soret Bands as a Distinctive Feature of High-Valent Transition Metal Corroles. *J. Am. Chem. Soc.* **2002**, *124*, 8104–8116.
(28) Ou, Z.; Shao, J.; Zhao, H.; Ohkubo, K.; Wasbotten, I. H.; Fukuzumi, S.; Ghosh, A.; Kadish, K. M. Spectroelectrochemical and ESR Studies of Highly Substituted Copper Corroles. *J. Porphyrins Phthalocyanines* **2004**, *08*, 1236–1247.
(29) Bröring, M.; Brégier, F.; Tejero, E. C.; Hell, C.; Holthausen, M. C. Revisiting the Electronic Ground State of Copper Corroles. *Angew. Chem., Int. Ed.* **2007**, *46*, 445–448.
(30) Alemayehu, A. B.; Gonzalez, E.; Hansen, L. K.; Ghosh, A. Copper Corroles Are Inherently Saddled. *Inorg. Chem.* **2009**, *48*, 7794–7799.
(31) Alemayehu, A. B.; Hansen, L. K.; Ghosh, A. Nonplanar, Noninnocent, and Chiral: A Strongly Saddled Metallocorrole. *Inorg. Chem.* **2010**, *49*, 7608–7610.
(32) Thomas, K. E.; Wasbotten, I. H.; Ghosh, A. Copper β-Octakis(Trifluoromethyl)Corroles: New Paradigms for Ligand Substituent Effects in Transition Metal Complexes. *Inorg. Chem.* **2008**, *47*, 10469–10478.
(33) Alemayehu, A. B.; Conradie, J.; Ghosh, A. A First TDDFT Study of Metallocorrole Electronic Spectra: Copper *meso*-Triarylcorroles Exhibit Hyper Spectra. *Eur. J. Inorg. Chem.* **2011**, *12*, 1857–1864.
(34) Berg, S.; Thomas, K. E.; Beavers, C. M.; Ghosh, A. Undecaphenylcorroles. *Inorg. Chem.* **2012**, *51*, 9911–9916.
(35) Thomas, K. E.; Vazquez-Lima, H.; Fang, Y.; Song, Y.; Gagnon, K. J.; Beavers, C. M.; Kadish, K. M.; Ghosh, A. Ligand Noninnocence in Coinage Metal Corroles: A Silver Knife-Edge. *Chem. – Eur. J.* **2015**, *21*, 16839–16847.
(36) Fang, Y.; Ou, Z.; Kadish, K. M. Electrochemistry of Corroles in Nonaqueous Media. *Chem. Rev.* **2017**, *117*, 3377–3419.
(37) Aartsma, T. J.; Gouterman, M.; Jochum, C.; Kwiram, A. L.; Pepich, B. V.; Williams, L. D. Porphyrins. 43. Triplet Sublevel Emission of Platinum Tetrabenzoporphyrin by Spectrothermal Principal Component Decomposition. *J. Am. Chem. Soc.* **1982**, *104*, 6278–6283.
(38) Baldo, M. A.; O'Brien, D. F.; You, Y.; Shoustikov, A.; Sibley, S.; Thompson, M. E.; Forrest, S. R. Highly efficient phosphorescent emission from organic electroluminescent devices. *Nature* **1998**, *395*, 151–154.
(39) Kwong, R. C.; Sibley, S.; Dubovoy, T.; Baldo, M.; Forrest, S. R.; Thompson, M. E. Efficient, Saturated Red Organic Light Emitting Devices Based on Phosphorescent Platinum(II) Porphyrins. *Chem. Mater.* **1999**, *11*, 3709–3713.
(40) Zach, P. W.; Freunberger, S. A.; Klimant, I.; Borisov, S. M. Electron-Deficient Near-Infrared Pt(II) and Pd(II) Benzoporphyrins with Dual Phosphorescence and Unusually Efficient Thermally Activated Delayed Fluorescence: First Demonstration of Simultaneous Oxygen and Temperature Sensing with a Single Emitter. *ACS Appl. Mater. Interfaces* **2017**, *9*, 38008–38023.
(41) Borisov, S. M.; Nuss, G.; Haas, W.; Saf, R.; Schmuck, M.; Klimant, I. New NIR-emitting complexes of platinum(II) and palladium(II) with fluorinated benzoporphyrins. *J. Photochem. Photobiol., A* **2009**, *201*, 128–135.
(42) Cebrián, C.; Mauro, M. Recent advances in phosphorescent platinum complexes for organic light-emitting diodes. *Beilstein J. Org. Chem.* **2018**, *14*, 1459–1481.
(43) Koszarna, B.; Gryko, D. T. Efficient Synthesis of *meso*-Substituted Corroles in a H_2O-MeOH Mixture. *J. Org. Chem.* **2006**, *71*, 3707–3717.
(44) Basato, M.; Biffis, A.; Martinati, G.; Tubaro, C.; Venzo, A.; Ganis, P.; Benetollo, F. Reaction of platinum acetate with phosphines and molecular structure of *trans*-$[Pt(OAc)_2(PPh_3)_2]$. *Inorg. Chim. Acta* **2003**, *355*, 399–403.
(45) *CELL_NOW: Index Twins and Other Problem Crystals*, version 2008/4; Bruker, 2016.
(46) Krause, L.; Herbst-Irmer, R.; Sheldrick, G. M.; Stalke, D. Comparison of silver and molybdenum microfocus X-ray sources for single-crystal structure determination. *J. Appl. Crystallogr.* **2015**, *48*, 3–10.
(47) *TWINABS: Bruker AXS Scaling for Twinned Crystals*, version 2012/1; Bruker, 2016.
(48) Sheldrick, G. M. SHELXT - Integrated Space-Group and Crystal-Structure Determination. *Acta Crystallogr., Sect. A: Found. Adv.* **2015**, *71*, 3–8.
(49) Sheldrick, G. M. Crystal Structure Refinement with SHELXL. *Acta Crystallogr., Sect. C: Struct. Chem.* **2015**, *71*, 3–8.
(50) Hübschle, C. B.; Sheldrick, G. M.; Dittrich, B. ShelXle: a Qt graphical user interface for SHELXL. *J. Appl. Crystallogr.* **2011**, *44*, 1281–1284.

DOI: 10.1021/acsomega.8b01149
ACS Omega 2018, 3, 9360–9368